

SMALL-CAPACITANCE JOSEPHSON JUNCTIONS: ONE-DIMENSIONAL ARRAYS AND SINGLE JUNCTIONS

MICHIO WATANABE

Semiconductors Laboratory, RIKEN (The Institute of Physical and Chemical Research), 2-1 Hirosawa, Wako-shi, Saitama 351-0198, Japan

DAVID B. HAVILAND

Nanostructure Physics, The Royal Institute of Technology (KTH), SCFAB, Roslagstullsbacken 21, 106 91 Stockholm, Sweden

I INTRODUCTION

Small-capacitance superconducting tunnel junctions provide an ideal system for studying the interplay between the Josephson phase and the charge on the junction electrode, which are quantum mechanically conjugate to each other. This interplay can be probed through the superconductor-insulator (SI) transition [1], which is a quantum phase transition occurring at $T = 0$. The SI transition has been extensively studied in two-dimensional (2D) systems. Experiments have been carried out on granular [2, 3, 4, 5] and homogeneous films [6, 7]. Theoretical studies have modeled the films as 2D arrays of small-capacitance Josephson junctions (JJs) [8, 9, 10, 11, 12], and experiments with such arrays have also been reported [13, 14]. In 1D, however, experimental study of the SI transition in JJ arrays has been less extensive, while the theoretical investigation has been done [1, 8, 15, 16, 17, 18, 19, 20]. Experimental data on long and narrow films are available [22, 21]. In contrast to films, JJ arrays can be fabricated with a

high degree of uniformity, and the parameters of interest in the theory can be measured. Furthermore, one can design a JJ array in such a way that one of the important parameter in the theory, the Josephson coupling energy E_J between adjacent islands can be tuned *in situ* [23, 24]. The other important parameters are the charging energy associated with the junction capacitance, $E_C \equiv e^2/2C$, and the stray capacitance of each island to the ground, $E_{C_0} \equiv e^2/2C_0$. Depending on the values of these parameters either superconducting or insulating behavior is expected for an array with infinite length.

In long arrays, it is possible to observe a well developed Coulomb blockade [25] for Cooper pairs in the current-voltage (I - V) characteristics, even when the Josephson energy is dominant, $E_J \geq E_C$. Such a Coulomb blockade is extremely interesting because our usual notions about phase coherence in the sense of the Josephson effect do not apply. The phase of the superconducting state is washed out by strong quantum fluctuations, and the number of Cooper pairs on the island becomes well defined. Nevertheless, the large Josephson coupling causes the potential associated with one excess Cooper pair to spread out, and in this sense the single excess Cooper pair becomes delocalized. In the Coulomb-blockade state, the single excess Cooper pair can be described as a charge soliton [26, 27], which is dual to the Josephson fluxon of 1D parallel arrays. The charge-soliton length, $\lambda_s = 2e/2\pi C_0 V_c$, gives the length scale over which the potential is screened. Here V_c is the critical voltage for Cooper-pair tunneling in a single junction, which is a function of the ratio E_J/E_C [28]. For $E_J \geq E_C$, V_c is reduced exponentially to zero as E_J increases. This weakening of the Coulomb blockade causes $\lambda_s \rightarrow \infty$, and we expect the insulating state of the array to eventually give way to superconductivity when $E_J \gg E_C$. In Sec. III, we describe experimental data which display this evolution of the insulating state as E_J is tuned *in situ*. We interpret the data qualitatively in terms of a theoretical model for a $T = 0$ quantum phase transition [1].

We have also used the 1D JJ arrays to bias a single Josephson junction in order to control the electromagnetic environment for the single junction [29]. In single junctions, experimental observation of Coulomb blockade has been considered to be extremely difficult because a high-impedance environment is necessary, and special care should be taken with the measurement leads [25]. For this reason, thin-film resistors [30] and tunnel-junction arrays [31, 32] were employed for the leads, and an increase of differential resistance around $V = 0$ was reported. In contrast to the earlier works [30, 31, 32], our leads are tunable, and we can therefore study the *same* single junction in different environments. We show that the I - V curve of the single junction is indeed sensitive to the state of the environment. Furthermore, we can induce a transition to a Coulomb blockade in the single junction when the zero-bias resistance of the JJ arrays is much higher than the quantum resistance $R_K \equiv h/e^2 \approx 26 \text{ k}\Omega$. In addition to Coulomb blockade, we have clearly observed a region of negative differential resistance in the I - V curve.

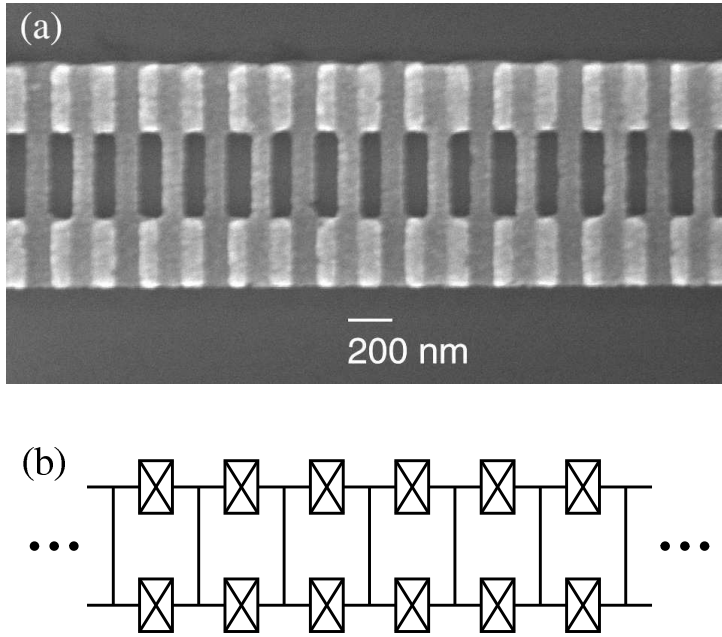


FIG. 1: One-dimensional array of small-capacitance dc SQUIDs. (a) Scanning electron micrograph. (b) Schematic diagram.

The negative differential resistance appears as a result of coherent tunneling of single Cooper pairs according to the theory of current-biased single Josephson junctions [25, 33]. Based on the theory, we have calculated the I - V curves numerically. The measured I - V is consistent with the numerical calculation.

II EXPERIMENT

A Sample fabrication and characterization

The 1D JJ arrays were fabricated on a SiO_2 substrate with electron-beam lithography and a double-angle-evaporation technique [34]. The arrays are made of Al with an Al_2O_3 tunnel barrier, and each of the Al electrodes in the array is connected to its neighbors by two junctions in parallel, thus forming a superconducting quantum interference device (SQUID) between nearest neighbors. Figure 1 shows a scanning electron micrograph of a section of an array and the schematic diagram. The advantage of the SQUID geometry is that we can control the effective E_J by applying an external magnetic field, B , perpendicular to the substrate,

$$E_J = E_{J0} \left| \cos \left(\pi \frac{BA_{\text{loop}}}{\Phi_0} \right) \right|, \quad (1)$$

where A_{loop} is the effective area of the SQUID loop and $\Phi_0 \equiv h/2e = 2 \times 10^{-15}$ Wb is the superconducting flux quantum. Because the geometrical inductance of the SQUID loop, $L_0 \ll$

$\Phi_0/2\pi I_{c0}$, an external magnetic field creates a phase shift so that the critical current between nearest neighbors is modulated in a periodic way. Here,

$$E_{J0} \equiv \left(\frac{\Phi_0}{2\pi} \right) I_{c0} \quad (2)$$

and

$$I_{c0} \equiv \frac{\pi\Delta_0}{2eR_n} \quad (3)$$

is the Ambegaokar-Baratoff critical current [35], which is calculated from the superconducting energy gap, Δ_0 ($= 0.2$ meV for Al), and normal-state tunnel resistance of the junction, R_n . Henceforth, we will refer to the lumped SQUID as an effective junction with a tunable E_J , and a fixed charging energy $E_C \equiv e^2/2C$, where C is the sum (parallel combination) of two junction capacitances.

There are a couple of ways to obtain R_n . The resistance of the array divided by the number of junctions, N , measured above the superconducting transition temperature, T_c ($= 1.2$ K for Al), or in a magnetic field strong enough to completely suppress the superconductivity (> 0.1 T for Al), is R_n by definition. It is also possible to find R_n by taking the slope of the I - V curve at high bias, $V > N(2\Delta_0/e)$. The capacitance $C = c_s A$ is estimated from the junction area A , where the specific capacitance c_s is on the order of 10^2 fF/ μm^2 as we will see later in Sec. IV.D. Another important parameter of the array is the capacitance of each electrode to the ground, $C_0 \sim 10$ aF [36], which depends on N logarithmically. In Sec. III, we will discuss three arrays with nominally identical junction parameters [$R_n = 4.9$ k Ω , $A = (0.4 \times 0.1 \mu\text{m}^2) \times 2$, and $A_{\text{loop}} = 0.7 \times 0.2 \mu\text{m}^2$], but having a different N : 255, 127, and 63.

The samples for Sec. IV.C and D are single Josephson junctions biased with the SQUID arrays. (See Fig. 2.) The single junction, which is in the center of Fig. 2a, has an area of $0.1 \times 0.1 \mu\text{m}^2$. On each side of the single junction there are two leads enabling four-point measurements of the single junction. A part of each lead close to the single junction consists of the SQUID array with $A = (0.3 \times 0.1 \mu\text{m}^2) \times 2$, and $A_{\text{loop}} = 0.7 \times 0.2 \mu\text{m}^2$. The samples are characterized by R_n , N , and the normal-state tunnel resistance of the single junction, r_n .

B Low-temperature measurements

The I - V curves and the zero-temperature resistance were measured in a ^3He - ^4He dilution refrigerator at $0.02 - 1$ K. The temperature was determined by measuring the resistance of a ruthenium-oxide thermometer [37] fixed at the mixing chamber. Special care was taken to filter the sample from high-frequency electromagnetic radiation [34]. The preamplifier stage of our measurement scheme was specially designed for the high resistances associated with the Coulomb blockade.

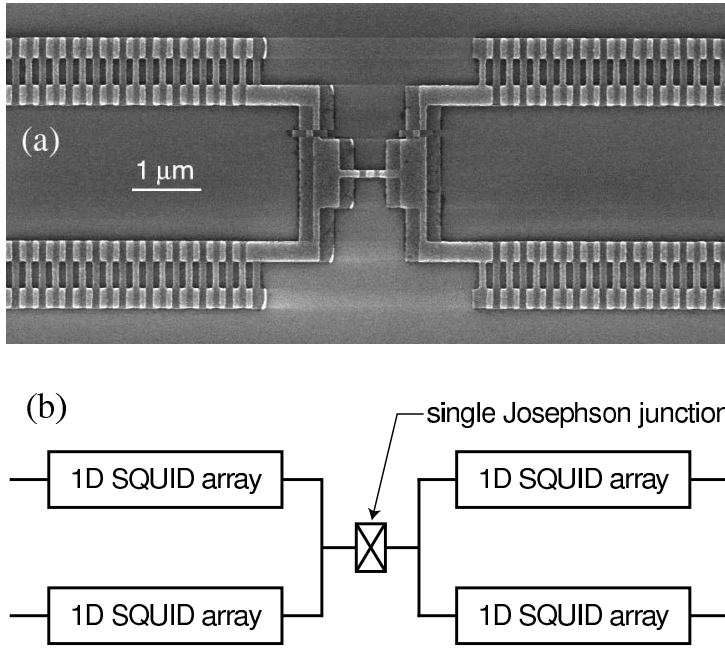


FIG. 2: Single Josephson junction biased with arrays of small-capacitance dc SQUIDs. (a) Scanning electron micrograph. (b) Schematic diagram.

The temperature dependence of the zero-bias resistance (Fig. 4) was determined with lock-in technique at 13 Hz [23]. The power dissipation was kept at 10^{-16} W, which was just large enough to yield a detectable signal, and at the same time, small enough to probe the “linear” response.

The I - V curve of the single junction (Fig. 9) were measured in a four-point configuration, where the potential difference was measured through one pair of SQUID-array leads with a high-input-impedance instrumentation amplifier, and through the other pair of SQUID-array leads, the bias was applied and the current was measured with a current preamplifier [29]. When the voltage drop at the SQUID arrays was much larger than that at the single junction, the single junction was practically current biased. The SQUID arrays could be measured in a two-point configuration (same current and voltage leads) on the same side of the single junction. Note that the two arrays are connected in series and that current does not flow through the single junction.

III SUPERCONDUCTOR-INSULATOR TRANSITION IN ONE-DIMENSIONAL ARRAYS

A Current-voltage characteristics and the zero-bias resistance

Figure 3a shows the I - V curve of the three arrays at zero magnetic field. The arrays were made

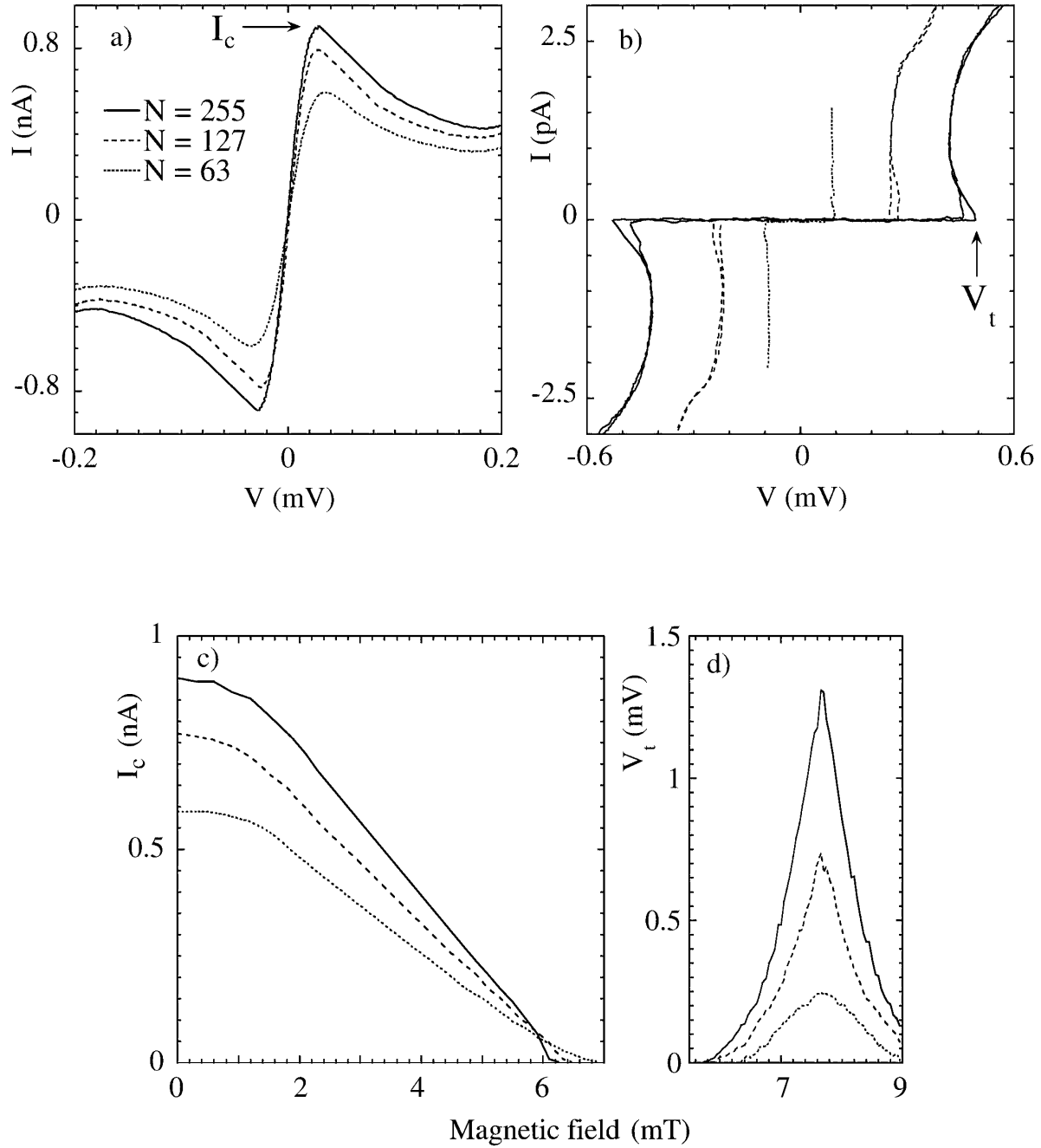


FIG. 3: Dependence of the I - V curves on the array length N , at $T = 0.05$ K. (a) The I - V curves at $B = 0$ showing Josephson-like behavior and the critical current I_c . (b) The I - V curves at $B = 7.1$ mT showing the Coulomb blockade of Cooper-pair tunneling and the threshold voltage V_t . (c) The magnetic field dependence of I_c . (d) The magnetic field dependence of V_t .

on the same chip, in the same vacuum cycle, using masks written to the same dimensions. Thus, all junctions in each array should be identical. The arrays are not truly superconducting, and there is actually a slope on the “zero-voltage” branch of the I - V curve, which gives a finite resistance. Furthermore, the observed “critical currents,” i.e., the first local current maximum at ≈ 0.03 mV, are only 1% of the classical Ambegaokar-Baratoff value. This critical current shows a clear dependence on the array length. The longer the array, the larger the critical current, indicating that superconducting behavior is favored in the longer array. As E_J is suppressed below E_{J0} with an externally applied magnetic field, the measured critical current of each array is reduced, and the resistance on the “zero-voltage” branch increases. Figure 3c shows the magnetic-field dependence of the critical current. In the neighborhood of $B_c = 5.8$ mT, the curves in Fig. 3c cross one another, so that for $B > B_c$, the longer the array, the smaller the critical current.

Figure 3b shows the I - V curve of the three arrays at $B = 7.1$ mT ($> B_c$). Here we see a new type of behavior which is dual to the $B < B_c$ behavior. The I - V curve is characterized by a zero-current state for voltage below a threshold voltage, where the array switches to a finite current state. The magnetic-field dependence of the threshold voltage for $B > B_c$ is shown in Fig. 3d for the three arrays. We see that the longer the array, the larger the threshold voltage, indicating that insulating behavior is favored in the longer array.

Figure 4 shows the temperature dependence of the zero-bias resistance, $R_0(T)$, taken at the same magnetic fields (same E_J) for two arrays of different length: $N = 255$ (solid) and 63 (dashed). Each set of the curves shows qualitatively similar behavior. At zero magnetic field, as the temperature is lowered R_0 decreases to a value which is temperature independent. As the magnetic field is increased, the resistance of this “flat tail” increases, until it reaches a critical value, where $R_0(T)$ curves make a sharp turn to increasing resistance as $T \rightarrow 0$. Further increasing of the magnetic field drives the array into the insulating state, where R_0 increases rapidly as $T \rightarrow 0$.

If we examine the bottom two curves in each set of Fig. 4, we can see that at high temperatures, the 63-junction array has a smaller resistance than the 255-junction array, as expected for a classical resistor. However, at low temperatures, the resistance of the 63-junction array becomes *larger* than the 255-junction array. This increasing of the resistance for shorter arrays is a clear sign that quantum fluctuations are responsible for the measured resistance [1]. The open circles in Fig. 4 indicate the crossing points where R_0 is the same for two different lengths at the same magnetic field. This crossing point moves towards $T = 0$ as the magnetic field is tuned to the critical point K_0^* . At the critical point, the $T \rightarrow 0$ resistance due to quantum fluctuations, is independent of the array length.

We have seen a magnetic-field-tuned transition from Josephson-like behavior to Coulomb

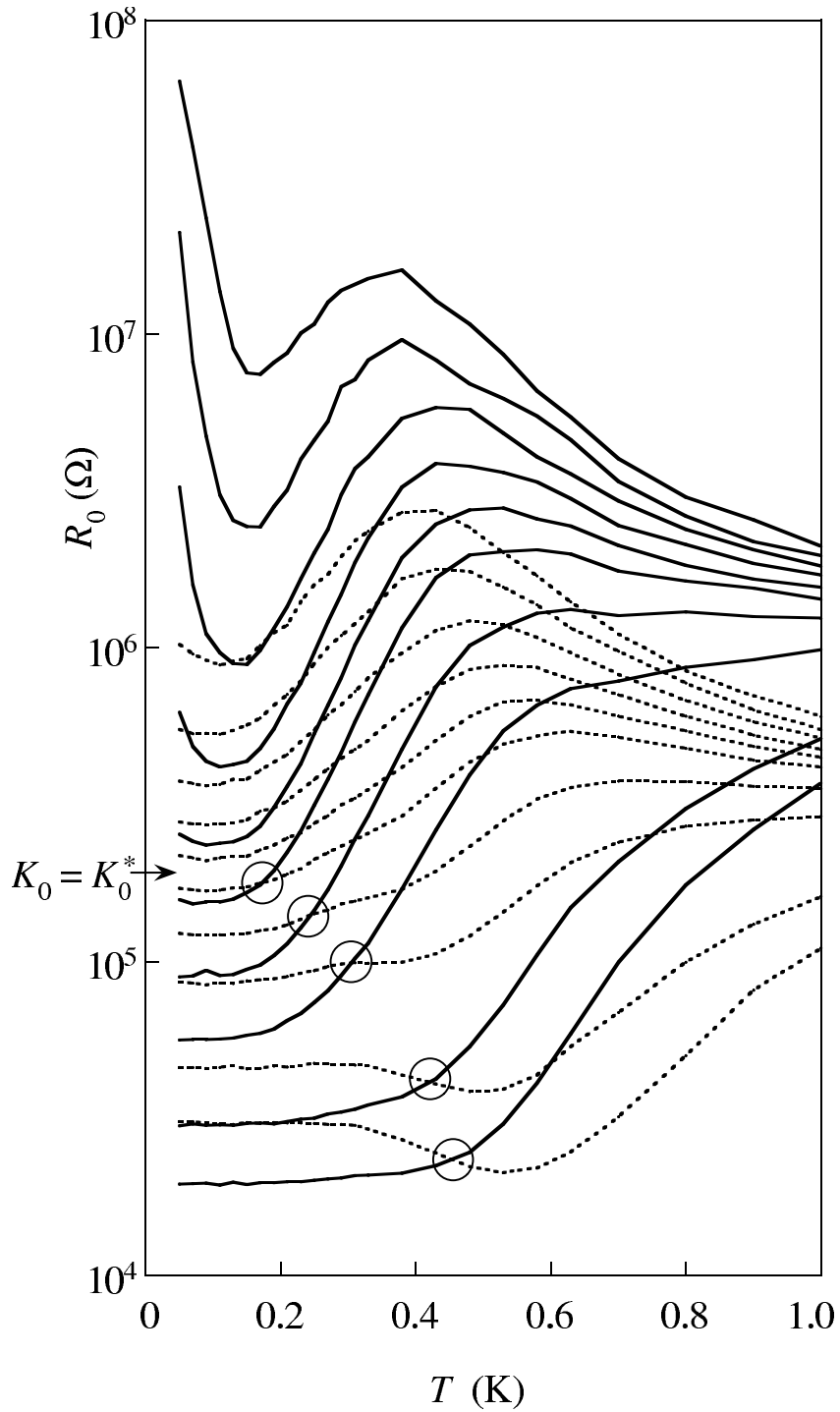


FIG. 4: Zero-bias resistance vs. temperature for two arrays having different number of junctions, N , but otherwise identical parameters. The set of solid curves are for $N = 255$ and the dashed curves are for $N = 63$, taken at the same magnetic fields between 0 and 7 mT. The open circles show where the measurements on the two arrays at the same magnetic field cross. At the magnetic field where $K_0 = K_0^*$, the two arrays have the same $T \rightarrow 0$ resistance, which is presumably independent of N .

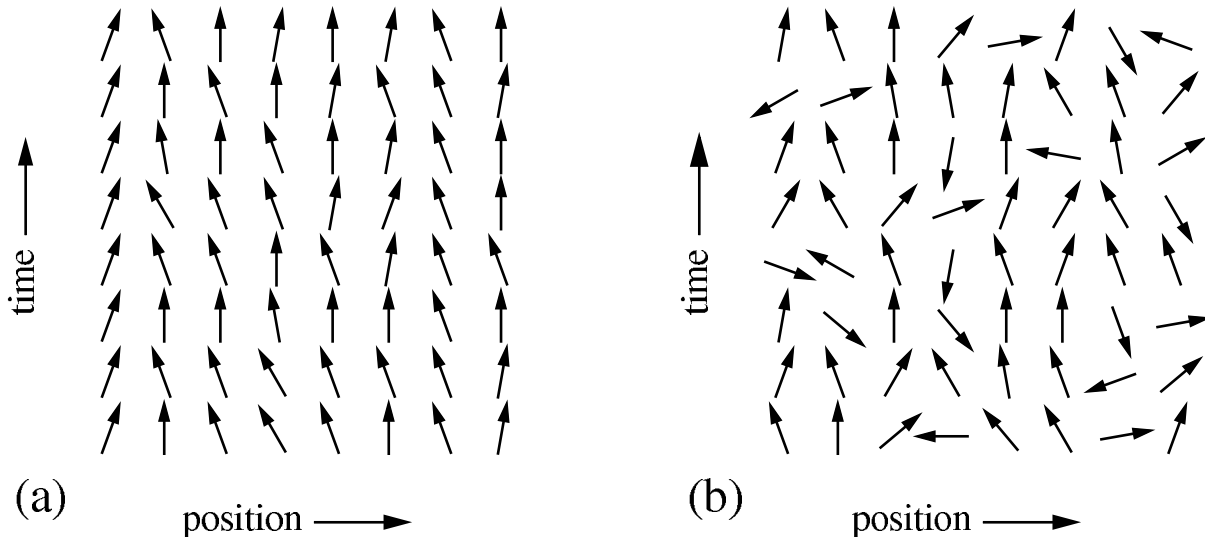


FIG. 5: Typical path or time history of a one-dimensional Josephson-junction array in (a) the superconducting phase and in (b) the insulating phase, respectively. The orientation of the arrows indicates the phase angles of the superconducting order parameter on the metallic elements connected by the Josephson junctions.

blockade, which may be called a superconductor-insulator transition, through the I - V curve (Fig. 3) and the temperature dependence of R_0 (Fig. 4). Moreover, the sharpness of the transition is strongly influenced by the length of the array. We can find qualitative explanation for this length dependence in a theoretical model of a quantum phase transition, which will be discussed in the following subsection.

B Mapping to the XY model

The SI transition can be described in an elegant theoretical framework as a quantum phase transition [1]. In these models, one can describe how a $T = 0$ property of a macroscopic quantum system with many degrees of freedom, will change as the complementary energies in the Hamiltonian of the system are adjusted. One can calculate the linear response, which in our case is the zero bias-resistance R_0 , resulting from quantum fluctuations of the degrees of freedom. Within this framework, our 1D quantum system of Josephson junctions is mapped to the classical XY model of (1+1)D as sketched in Figs. 5a and 5b, the extra dimension being imaginary time, $i\hbar/k_B T$. Note that the role of temperature for the quantum system is to set the “size” of the system in the imaginary-time dimension. The (1+1)D classical XY model exhibits a Berzinski-Kosterlitz-Thouless phase transition [38, 39], from a disordered state (free vortices) to an ordered state (bound vortex pairs) as the strength of the dimensionless coupling constant, K_0 is increased. The quantum fluctuations of the phase of the superconducting wave

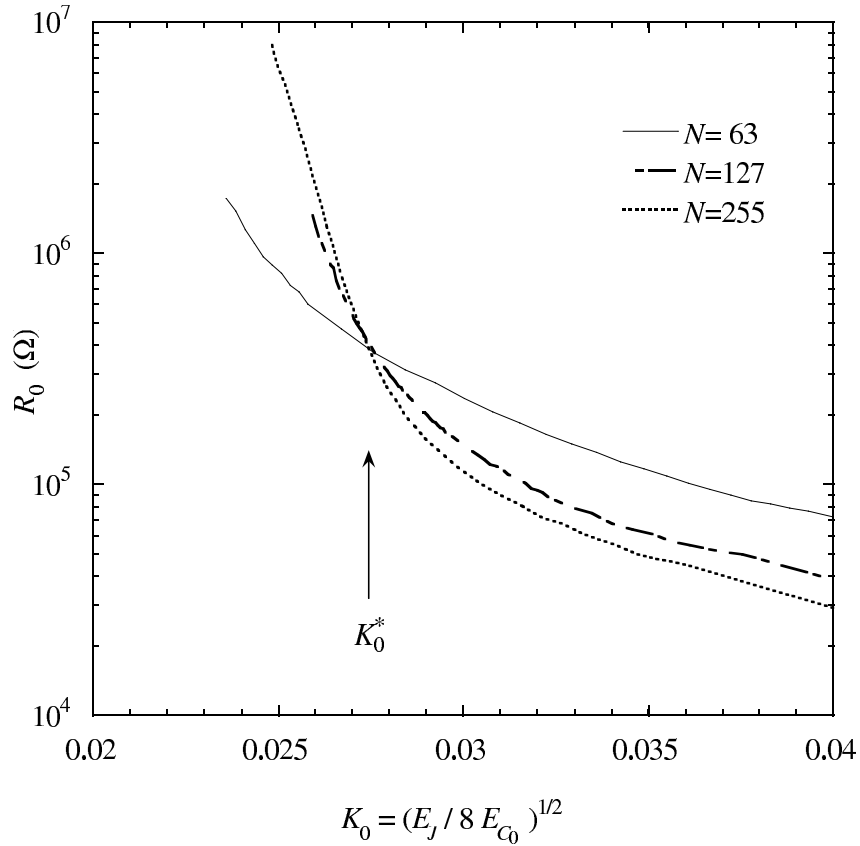


FIG. 6: Zero-bias resistance taken at $T = 0.05$ K as a function of the dimensionless coupling constant $K_0 = (E_J/8E_{C_0})^{1/2}$ for three arrays having different number of junctions.

function are thus described in terms of vortices, and in the insulating state (large quantum fluctuations) corresponds to the free-vortex state of the XY model [40]. The mapping to the isotropic XY model [15] can be done in the limit $C_0 \gg C$ which results in $K_0 = (E_J/8E_{C_0})^{1/2}$, where $E_{C_0} = e^2/2C_0$ is the charging energy associated with the stray capacitance of each electrode. Thus in this mapping, the junction capacitance, C is neglected.

Figure 6 shows a plot of R_0 measured at the lowest temperature, $T = 0.05$ K, vs. $K_0 = (E_J/8E_{C_0})^{1/2}$ for three arrays with $N = 255, 127$ and 63 . We see in Fig. 6 that the three curves for different lengths cross at nearly the same point, $K_0^* = 0.027$. To the left of this crossing point we have the insulating state, where the resistance is larger for the longer arrays. To the right of this crossing point, we have the superconducting state, where the resistance is *smaller* for longer arrays. The arrays in the experiments have $C \gg C_0$, and thus we can not directly apply the theory. In our earlier work [23] we postulated that the effect of $C \gg C_0$ could be accounted for by “course graining” to the scale $\Lambda = (C/C_0)^{1/2}$, which would result in a coupling constant $J = (E_J/\Lambda E_C)^{1/2}$. Figure 4 of Ref. [23] shows that for this choice of the dimensionless coupling

constant, the R_0 vs. J curves do not cross at the same point, but in the region $J \in \{0.49, 0.55\}$. Choi *et al.* [20] have made a theoretical analysis of the role of a finite junction capacitance C by treating Λ as a small parameter. They found that the transition point should approach the limiting value $K_0^c = 2/\pi = 0.64$ when extrapolated to large Λ . The fact that the curves cross at one point in Fig. 6 would suggest that $K_0 = (E_J/8E_{C_0})^{1/2}$ is indeed the correct parameter for the transition. However, the experiment does not support the conclusions of Choi *et al.* in that the experimental critical point $K_0^* \approx 0.03 \ll K_0^c = 2/\pi$.

As we have seen earlier in Fig. 4, the resistance at $T > 0.6$ K is almost proportional to the array length, and in this sense, the arrays behave like classical 1D resistors. At lower temperatures, however, large deviations from this classical behavior occur. We can qualitatively understand these observations in the context of the (1+1)D XY model by considering the finite-size effect, which plays an important role in a real experiment. The zero-bias resistance of the array is determined by quantum fluctuations of the superconducting phase, which are described by the vortices in the (1+1)D XY model. As the temperature is lowered, the system becomes larger in the imaginary-time dimension, and at low enough temperatures, the system size in the real-space dimension, or the array length, determines the energy for free-vortex formation. The energy increases with increasing system size, and thus the probability of free-vortex formation is reduced in a longer array. This means that in a longer array, the superconducting state is favored. If we assume that the zero-bias resistance of the array is proportional to the probability of free-vortex formation in the isotropic XY model with the area of N^2 (i.e., N units in real space and N units in imaginary time), we obtain

$$R_0 \sim N^{2-\pi K_0} \quad (4)$$

by neglecting any renormalization effects [41]. For $K_0 > K_0^c = 2/\pi$, R_0 increases for decreasing N , as observed in Fig. 4 on the superconducting side of the transition.

IV COULOMB BLOCKADE IN SINGLE JUNCTIONS

A Theory for current-biased single Josephson junctions

The Hamiltonian of a single Josephson junction in an environment with sufficiently high impedance is written as

$$H = \frac{Q^2}{2C} - E_J \cos \phi, \quad (5)$$

where Q is the charge on the junction electrode, C is the capacitance of the junction, E_J is the Josephson energy, and ϕ is the Josephson-phase difference across the junction. The charge Q and $\hbar\phi/2e$ are quantum mechanically conjugate variables, and a set of the eigenfunctions are

Bloch waves of the form

$$\Psi(\phi) = u(\phi) \exp(i\phi q/2e), \quad (6)$$

where q is called quasicharge and $u(\phi)$ is a periodic function,

$$u(\phi + 2\pi) = u(\phi). \quad (7)$$

The energy eigenvalue E plotted as a function of q has a band structure, and in all the allowed bands, it is $2e$ periodic. An example of the energy diagram for $E_J/E_C = 0.2$, where $E_C \equiv e^2/2C$ is the charging energy, is shown in Fig. 7a. Under constant current bias I_x , in the absence of quasiparticle or Cooper-pair tunneling, q increases uniformly in time according to

$$\frac{dq}{dt} = I_x \quad (8)$$

so that the state of the system advances toward higher q within a given band as time goes on. The average voltage is given by

$$\langle V \rangle = \sum_{i_b, q} P(i_b, q) \frac{dE(i_b, q)}{dq}, \quad (9)$$

where i_b is the band index and $P(i_b, q)$ is the probability that the system is in the state (i_b, q) . The probability $P(i_b, q)$ can be calculated by solving a set of coupled differential equations of the form

$$\frac{dP(i_b, q)}{dt} = \sum_{i'_b, q'} A(i_b, q, i'_b, q') P(i'_b, q') = 0, \quad (10)$$

where the matrix element $A(i_b, q, i'_b, q')$ describes the rate of transition between the states (i_b, q) and (i'_b, q') . The dominant process for $A(i_b, q, i'_b, q')$ depends on the magnitude of I_x .

An example of the theoretical I - V curve is shown in Fig. 7b. For sufficiently small I_x (region CB), the dominant process is stochastic quasiparticle tunneling, where q changes by e . This tunneling always occurs along the energy parabola $q^2/2C$, such that i_b changes by 0 or ± 1 if the initial state is in the lowest band ($i_b = 1$) and by ± 1 for all the other initial states ($i_b \geq 2$) [33]. The rate for the quasiparticle tunneling is given by

$$\Gamma(\Delta E) = \frac{\Delta E / e^2 R_{\text{qp}}}{\exp(\Delta E / k_B T) - 1}, \quad (11)$$

where R_{qp} is the quasiparticle resistance and ΔE is the difference in energy between the initial (i_b, q) and final (i'_b, q') states,

$$\Delta E \equiv E(i'_b, q') - E(i_b, q). \quad (12)$$

At sufficiently low temperatures, the tunneling with $\Delta E > 0$ is extremely unfavorable, and the I - V curve is highly resistive (Coulomb blockade). For larger I_x (region BO in Fig. 7b), the

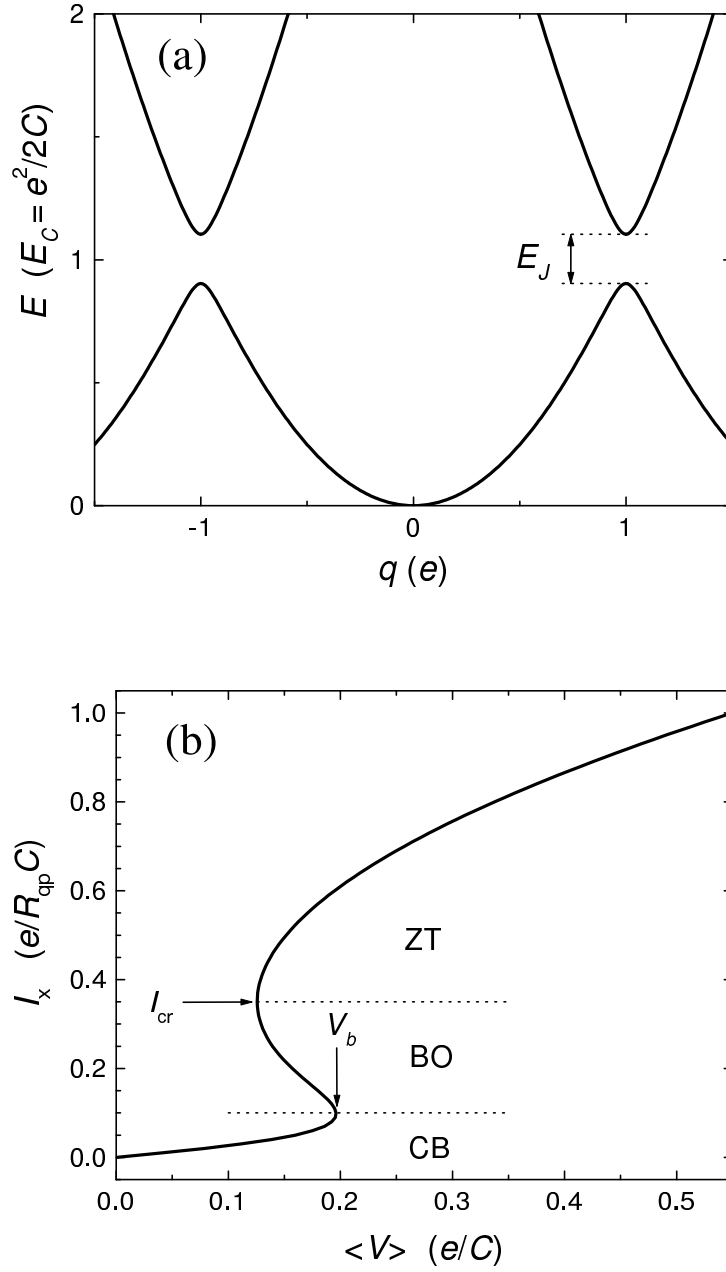


FIG. 7: (a) Energy diagram and (b) theoretical current-voltage characteristics for a single Josephson junction with $E_J/E_C = 0.2$ and $R_{qp} = 200 (h/\pi^2 e^2)$ at $k_B T/E_C = 0.2$, where E_J is the Josephson energy, $E_C \equiv e^2/2C$ is the charging energy, R_{qp} is the quasiparticle resistance, and $k_B T$ is the thermal energy. (The energy diagram depends only on E_J/E_C .)

quasicharge is frequently driven to the boundary of the Brillouin zone, $q = e$, then taken to $-e$ as a Cooper pair tunnels (Bloch oscillation). This process decreases $\langle V \rangle$, and as a result, the I - V curve has a region of negative differential resistance, or “back bending” in the low-current part. For still larger I_x (region ZT in Fig. 7b), Zener tunneling becomes important, and $\langle V \rangle$ increases again. In Zener tunneling, no quasicharge is transferred but the state of the system jumps from one band to another as it passes by the narrow gap between the bands. The probability of Zener tunneling from band i_b to $i_b + 1$ or vice versa is given by

$$P_Z = \exp \left[-\frac{\pi}{8} \frac{(\Delta E)^2}{i_b E_C} \frac{e}{\hbar I_x} \right]. \quad (13)$$

Following Ref. [42] which takes into account the above tunneling processes (quasiparticle, Cooper-pair, and Zener), we have calculate the I - V curve numerically. The parameters for the calculation are E_J/E_C , $k_B T/E_C$, and $\alpha \equiv h/\pi^2 e^2 R_{\text{qp}}$. The current and the voltage are in units of $e/R_{\text{qp}}C$ and e/C , respectively.

As we have seen in Fig. 7b, a typical I - V curve consists of three regions, so that it is characterized by the local voltage maximum, or blockade voltage V_b , and the local current minimum, or crossover current I_{cr} . (Here, we have to mention that the back-bending feature is smeared out if $k_B T/E_C$ or α is increased considerably.) Analytic expression of V_b and I_{cr} has been obtained theoretically for limiting cases [33]. The value of V_b is a function of E_J/E_C , and given by

$$V_b \approx \begin{cases} 0.25 e/C & \text{for } E_J/E_C \ll 1, \\ \delta_0/e & \text{for } E_J/E_C \gg 1, \end{cases} \quad (14)$$

as $T \rightarrow 0$, where

$$\delta_0 = \frac{e^2}{C} 8 \left(\frac{1}{2\pi^2} \right)^{1/4} \left(\frac{E_J}{E_C} \right)^{3/4} \exp \left[-\left(8 \frac{E_J}{E_C} \right)^{1/2} \right] \quad (15)$$

is the half width of the lowest energy band. As for I_{cr} ,

$$I_{\text{cr}} \sim \left(I_Z \frac{e}{R_{\text{qp}}C} \right)^{1/2} \quad (16)$$

is expected for $\alpha \ll (E_J/E_C)^2 \ll 1$ and $T \rightarrow 0$, where

$$I_Z \equiv \frac{\pi}{8} \frac{e E_J^2}{\hbar E_C} \quad (17)$$

is the Zener breakdown current. Note that I_{cr} is much smaller than I_Z . When we compare our experimental results with the theory, we need theoretical prediction for finite $k_B T/E_C$, and arbitrary E_J/E_C and α . For this reason we have done the numerical calculation. The measured V_b and I_{cr} will be compared with the calculation in Sec. IV.D.

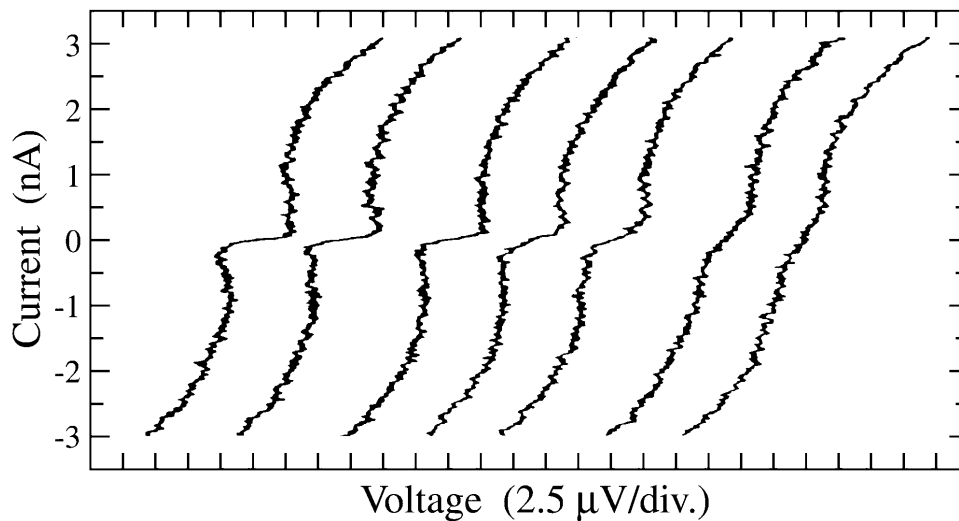


FIG. 8: Current-voltage characteristics of a single Josephson junction biased with thin-film resistors at several temperatures. From left to right, $T = 0.06, 0.08, 0.11, 0.17, 0.23, 0.28,$ and 0.34 K, respectively. The origin of the voltage axis is displaced for each curve for clarity.

B Earlier experiments on single junctions

In order to observe the Coulomb blockade in a single junction experimentally, the electromagnetic environment for the junction, or the measurement leads connected to the junction, should have a high impedance [25]. For this reason, thin-film resistors (NiCr alloy, AuPd alloy, Cr, and layered Ge/Pd) [30] and tunnel-junction (Al/Al₂O₃/Al) arrays [31, 32] were employed for the leads to bias a single junction (Al/Al₂O₃/Al).

Figure 8 shows the I - V curves of a single Josephson junction biased with thin-film resistors at several temperatures. A clear Coulomb blockade is seen at $T \leq 0.11$ K, and a “back bending” is also visible. In similar samples, high-frequency ($f = 0.4 - 10$ GHz) irradiation induced steps in the dc I - V curve at $I = \pm 2ef$ (not $\pm ef$), which can be explained as a phase locking of the externally applied signal to the Bloch oscillations [30].

Geerligs used 2D tunnel-junction arrays for the leads [31]. He claimed that in the normal state ($T > T_c$), a Coulomb blockade was visible in the single-junction I - V curve. In the superconducting state ($T < T_c$), however, neither the arrays nor the single junction develop clear charging effects, and the single junction showed a classic hysteretic I - V curve with an ordinary supercurrent. We believe that his arrays were in the superconducting side of the SI transition, and did not have high enough impedance below T_c .

Shimazu *et al.* biased a single junctions with 1D tunnel-junction arrays, and reported an increase of differential resistance around $V = 0$ in the normal state [32]. In the superconducting state, they measured the zero-bias resistance rather than the I - V curve. The zero-bias resistance

in the superconducting state was higher than the normal-state resistance for some single junctions, which suggests the existence of a Coulomb blockade even in the superconducting state. However, this increase of the zero-bias resistance could also be due to simple quasiparticle tunneling, which is independent of any Coulomb blockade effects for Cooper pairs.

C Single Josephson junctions biased with SQUID arrays

We have employed 1D arrays of dc SQUIDs for the leads to bias a single Josephson junction [29]. The advantage of this SQUID configuration is that in contrast to the earlier experiments in Sec. IV.B, the impedance can be varied *in situ* by applying an external magnetic field at low temperatures. (See Fig. 4.) Thus, we can tune the electromagnetic environment for the single junction over a wide range. In Figs. 9 and 10, we show some results on a sample with $r_n = 17 \text{ k}\Omega$, $R_n = 1.4 \text{ k}\Omega$, and $N = 65$. The I - V curves for the single junction at several normalized magnetic fields, $\varphi \equiv BA_{\text{loop}}/\Phi_0$, are shown in Fig. 9. As φ is varied, the I - V curve develops a Coulomb blockade. We emphasize that the Josephson energy of the single junction is independent of φ , because it does not have a SQUID configuration and the field $\varphi\Phi_0/A_{\text{loop}} < 7 \text{ mT}$ applied here is much smaller than the critical field for Al films ($\approx 0.1 \text{ T}$). The electromagnetic environment for the single junction (the SQUID array), however, is strongly varied with φ . The behavior of the single junction demonstrated in Fig. 9 does not result from the magnetic-field influencing the single-junction I - V curve, but rather from an environmental effect on the single junction. This experiment demonstrates in a direct way that the single-junction I - V curve is indeed sensitive to the electromagnetic environment.

The I - V curves of the two SQUID-array leads connected in series at $\varphi = 0.43$ ($R_0 = 0.61 \text{ M}\Omega$), 0.46 ($R_0 = 3.2 \text{ M}\Omega$), and 0.49 ($R_0 = 43 \text{ M}\Omega$) are shown in Fig. 10. The I - V curves of the leads are nonlinear, and in general the SQUID array cannot be described by a linear impedance model [24]. However, we may characterize the environment by their R_0 . Coulomb blockade is visible only when $R_0 \gg R_K$, which is consistent with the theoretical conditions for the clear observation of Coulomb blockade in single junctions [43]. For an arbitrary linear environment characterized by $Z_e(\omega)$, $\text{Re}[Z_e(\omega)] \gg R_K$ is required for the Coulomb blockade of quasiparticle tunneling and $\text{Re}[Z_e(\omega)] \gg R_K/4$ for that of Cooper-pair tunneling [43]. It is interesting to note that at $\varphi = 0.46$ (labeled “b”), the I - V curve of the leads is still “Josephson-like” (differential resistance is lower around $V = 0$), while that of the single junction is already “Coulomb-blockade-like”. This feature becomes more distinct in samples with larger N [44].

D Comparison with the numerical calculation

The region of negative differential resistance seen in Fig. 9 when Coulomb blockade is well developed, is related to coherent tunneling of single Cooper pairs according to the theory [25,

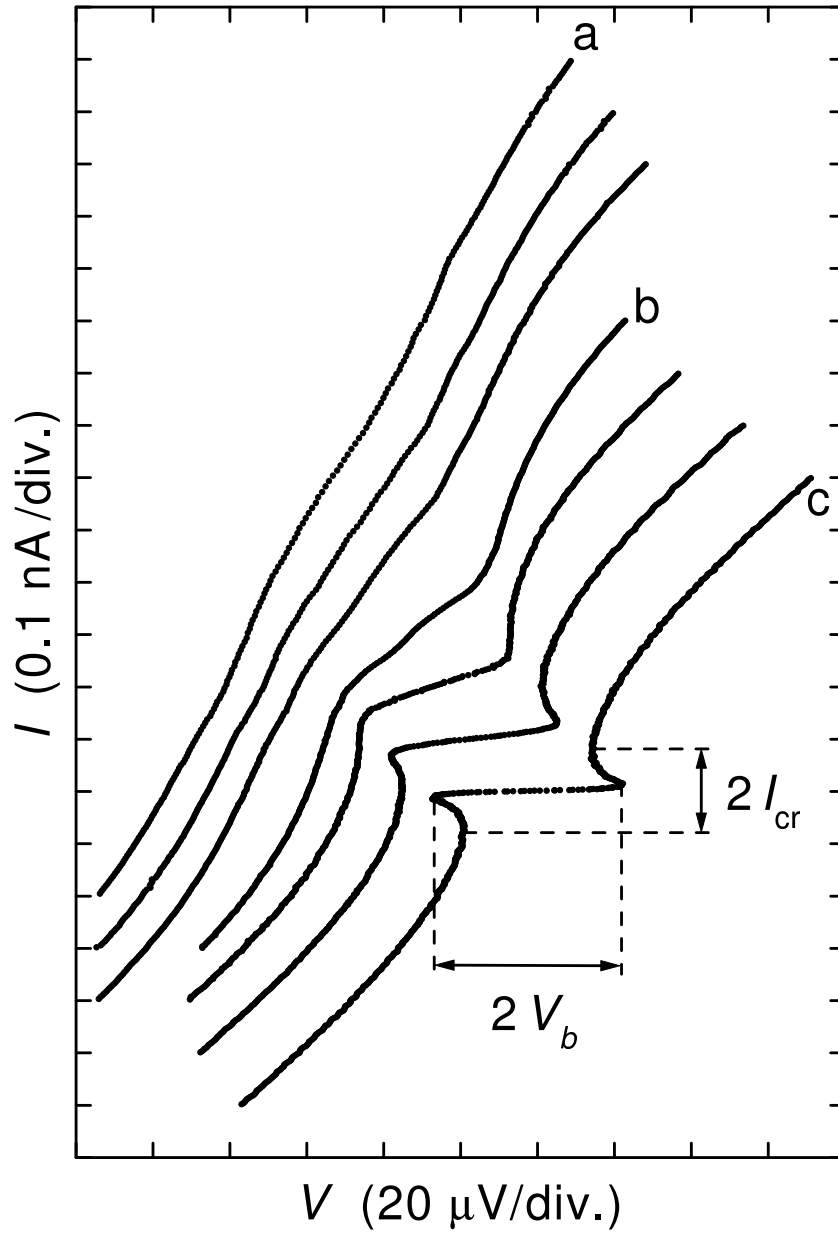


FIG. 9: Current-voltage (I - V) curves of the single junction at $T = 0.02$ K for a sample with $r_n = 17$ k Ω , $R_n = 1.4$ k Ω , and $N = 65$. From top left to bottom right, the normalized magnetic field $\varphi \equiv BA_{\text{loop}}/\Phi_0$ is increased from 0.43 to 0.49 in steps of 0.01. The origin of each curve is offset for clarity. For the labeled curves, the I - V characteristics of the leads at the same φ are shown in Fig. 10

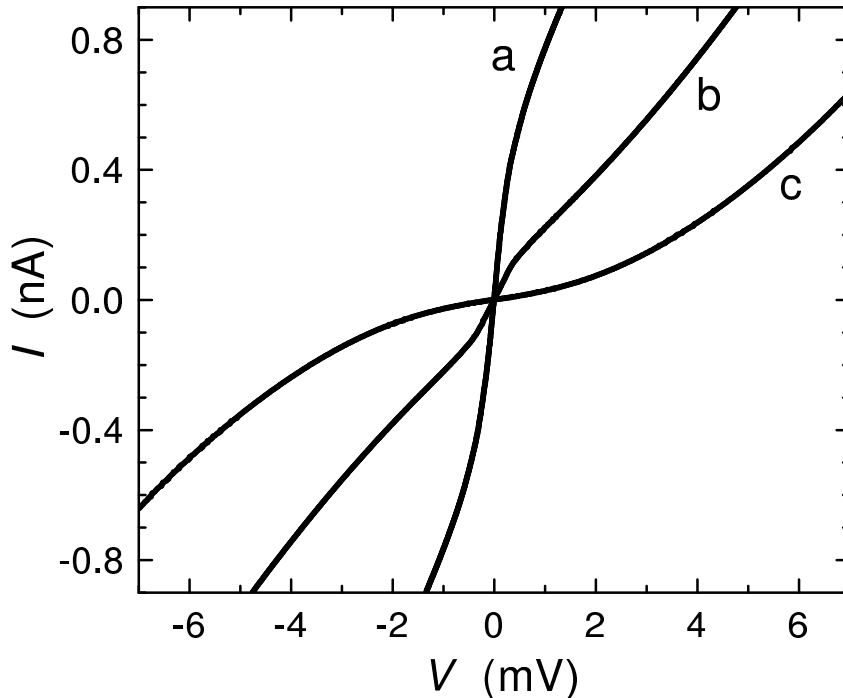


FIG. 10: Current-voltage curves of the two SQUID-array leads connected in series at $T = 0.02$ K for the same sample as in Fig. 9. From a to c, $\varphi \equiv BA_{\text{loop}}/\Phi_0$ is 0.43, 0.46, and 0.49, respectively.

33] of a current-biased single Josephson junction in an environment with sufficiently high impedance. Following Ref. [42], we have calculated the blockade voltage V_b numerically as a function of E_J/E_C [45]. The measured V_b (See Fig. 9) for the samples having nominal junction area of $0.1 \times 0.1 \mu\text{m}^2$ is compared with the numerical calculation in Fig. 11. The boxes and circles represent the samples biased with thin-film resistors (Sec. IV.B) and with SQUID arrays (Sec. IV.C), respectively. For the sample shown in Fig. 9, we used the data at $\varphi = 0.49$ (curve c) in order to obtain V_b . At $\varphi = 0.49$ the voltage drop at the SQUID arrays is 10^2 times larger than that at the single junction, and the single junction is therefore considered to be current biased. Compare the voltage scale of Figs. 9 and 10. We calculated E_J from r_n , $E_J = h\Delta_0/8e^2r_n$. For E_C , we employed $c_s = 130 \text{ fF}/\mu\text{m}^2$, and with this value the experimental data, especially those for the samples biased with SQUID arrays (the circles in Fig. 11), agree with the numerical calculation.

Actually, a smaller value, $c_s = 45 \pm 5 \text{ fF}/\mu\text{m}^2$ [46], which was obtained for the junctions with $3 \times 28 \mu\text{m}^2$ and $7 \times 54 \mu\text{m}^2$, has been frequently employed [23, 24, 30, 32, 36]. Our apparently large c_s may be partly explained by distributed capacitance of the SQUID arrays or by residual environmental effects. We also note that the uncertainty in c_s seems to be large when the junction area is on the order of $0.01 \mu\text{m}^2$ or smaller. For example, Fulton and Dolan measured

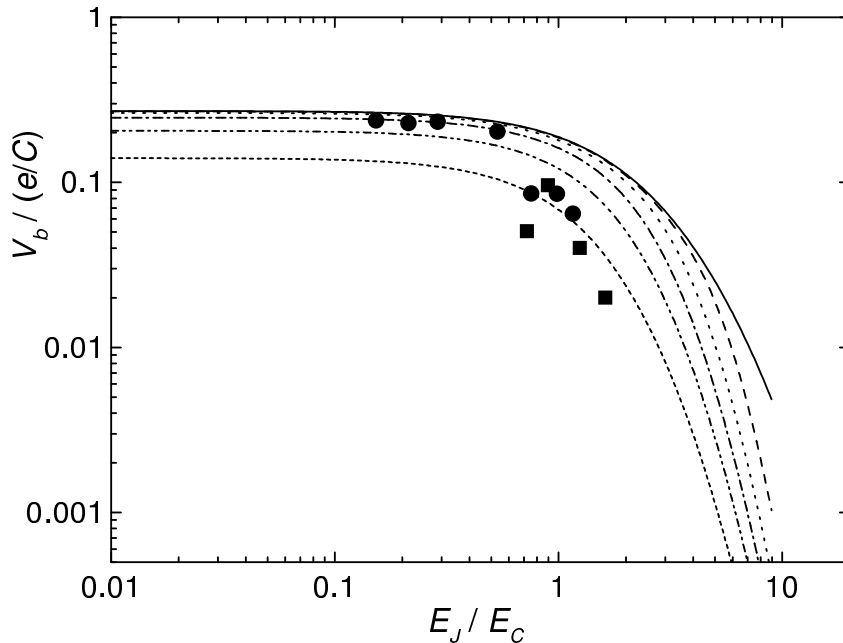


FIG. 11: Blockade voltage V_b divided by e/C as a function of E_J/E_C . From top to bottom, the curves represent the numerical calculations for normalized temperatures $k_B T/E_C = 0, 0.02, 0.05, 0.1, 0.2,$ and 0.5 , respectively.

samples with three junctions that share a common electrode, and obtained $0.20 - 0.23$ fF for $(0.03 \pm 0.01 \mu\text{m})^2 \times 3$ [47], i.e., $c_s = 42 - 192$ fF/ μm^2 . Geerligs *et al.* reported $c_s \approx 110$ fF/ μm^2 for two-dimensional (190×60) junction arrays with the areas of 0.01 or $0.04 \mu\text{m}^2$ [13]. More recently, Penttilä *et al.* studied resistively shunted single Josephson junctions with the area of $0.15 \times 0.15 \mu\text{m}^2$ [48]. The estimated C of their eight samples ranged between 0.8 and 6.6 fF, or $c_s = 36 - 293$ fF/ μm^2 .

When C is determined, it is possible to estimate R_{qp} of the samples from I_{cr} . We plot the measured I_{cr} for the single junctions biased with SQUID arrays (Sec. IV.C) as a function of E_J/E_C together with some theoretical curves based on our numerical calculation in Fig. 12. We obtain $R_{\text{qp}} = 10^0 - 10^1$ M Ω , or $R_{\text{qp}}/r_n = 10^2 - 10^3$.

V CONCLUSIONS

One-dimensional (1D) arrays of small-capacitance SQUIDs undergo a sharp transition, from Josephson-like behavior to the Coulomb blockade of Cooper-pair tunneling, as the effective Josephson coupling between nearest neighbors is tuned with an externally applied magnetic field. We have shown how length scaling of the zero-bias resistance of the array can be used to probe the superconductor-insulator quantum phase transition. The observed non-classical

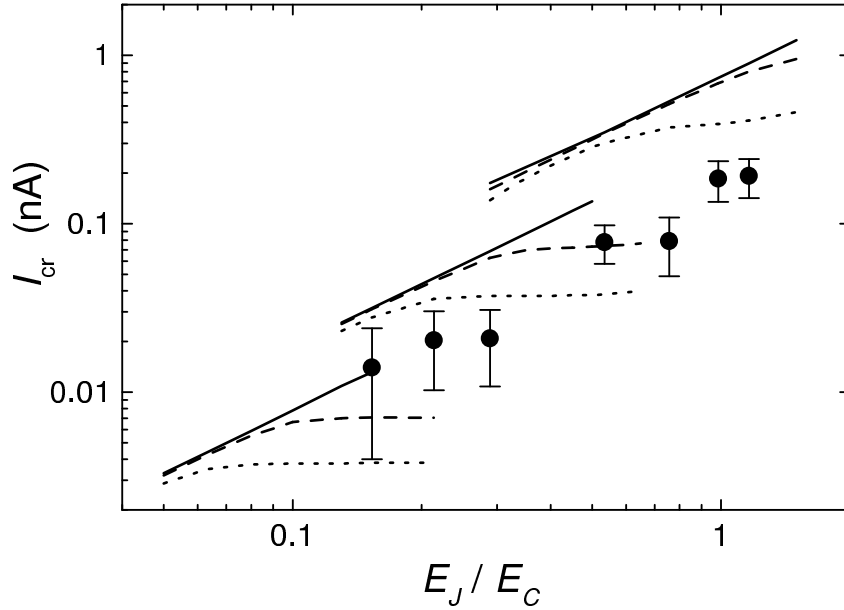


FIG. 12: Crossover current I_{cr} vs. E_J/E_C . The curves represent the numerical calculations for $C = 1.3$ fF, and from top to bottom $(\alpha \equiv h/\pi^2 e^2 R_{\text{qp}}, k_B T/E_C) = (10^{-2}, 0), (10^{-2}, 0.3), (10^{-2}, 0.5), (10^{-3}, 0), (10^{-3}, 0.3), (10^{-3}, 0.5), (10^{-4}, 0), (10^{-4}, 0.3),$ and $(10^{-4}, 0.5)$, respectively.

dependence of the zero-bias resistance on the length of the array, where the zero-bias resistance decreases with increasing length, can be supported qualitatively with a theoretical model which maps a 1D quantum system to the $(1+1)$ D classical XY model.

We have also used the SQUID arrays as a tunable electromagnetic environment for a single small-capacitance Josephson junction, and demonstrated how the Coulomb blockade of Cooper-pair tunneling is induced in the single junction. When the Coulomb blockade is well developed, the measured current-voltage curve is consistent with the numerical calculation for a current-biased single Josephson junction.

ACKNOWLEDGMENTS

We are grateful to R. L. Kautz for great help in the numerical calculation, and to T. Kato and F. W. J. Hekking for fruitful discussions. This work was supported by Swedish NFR, and Special Postdoctoral Researchers Program and President's Special Research Grant of RIKEN. The samples for Sec. III were fabricated at the Swedish Nanometer Laboratory. M. W. would like to thank the Japan Society for the Promotion of Science (JSPS) and the Swedish Institute (SI) for financial support.

REFERENCES

- [1] S. L. Sondhi, S. M. Girvin, J. P. Carini, and D. Shahar, *Rev. Mod. Phys.* **69**, 315 (1997).
- [2] H. M. Jaeger, D. B. Haviland, B. G. Orr, and A. M. Goldman, *Phys. Rev. B* **40**, 182 (1989).
- [3] A. F. Hebard and M. A. Paalanen, *Phys. Rev. Lett.* **65**, 927 (1990).
- [4] R. P. Barber, Jr. and R. C. Dynes, *Phys. Rev. B* **48**, 10618 (1993).
- [5] M. Watanabe, H. Shimada, S. Kobayashi, and Y. Ootuka, *J. Phys. Soc. Jpn.* **66**, 1419 (1997).
- [6] Y. Liu, D. B. Haviland, B. Nease, and A. M. Goldman, *Phys. Rev. B* **47**, 5931 (1993).
- [7] J. M. Valles, Jr., R. C. Dynes, and J. P. Garno, *Phys. Rev. Lett.* **69**, 3567 (1992).
- [8] M.-C. Cha, M. P. A. Fisher, S. M. Girvin, M. Wallin, and A. P. Young, *Phys. Rev. B* **44**, 6883 (1991).
- [9] A. P. Kampf and G. T. Zimanyi, *Phys. Rev. B* **47**, 279 (1993).
- [10] E. Šimánek, *Phys. Lett. A* **177**, 367 (1993).
- [11] A. van Otterlo, K.-H. Wagenblast, R. Fazio, and G. Schön, *Phys. Rev. B* **48**, 3316 (1993).
- [12] M. Wallin, E. S. Sørensen, S. M. Girvin, and A. P. Young, *Phys. Rev. B* **49**, 12115 (1994).
- [13] L. J. Geerligs, M. Peters, L. E. M. de Groot, A. Verbruggen, and J. E. Mooij, *Phys. Rev. Lett.* **63**, 326 (1989).
- [14] C. D. Chen, P. Delsing, D. B. Haviland, Y. Harada, and T. Claeson, *Phys. Rev. B* **51**, 15645 (1995).
- [15] R. M. Bradley and S. Doniach, *Phys. Rev. B* **30**, 1138 (1984).
- [16] S. E. Korshunov, *Euro. Phys. Lett.* **9**, 107 (1989).
- [17] P. A. Bobbert, R. Fazio, G. Schön, and A. D. Zaikin, *Phys. Rev. B* **45**, 2294 (1992).
- [18] A. A. Odintsov, *Phys. Rev. B* **54**, 1228 (1996).
- [19] L. I. Glazman and A. I. Larkin, *Phys. Rev. Lett.* **79**, 3736 (1997).
- [20] M.-S. Choi, J. Yi, M. Y. Choi, J. Choi, and S.-I. Lee, *Phys. Rev. B* **57**, R716 (1998).
- [21] A. V. Herzog, P. Xiong, F. Sharifi, and R. C. Dynes, *Phys. Rev. Lett.* **76**, 668 (1996).
- [22] F. Sharifi, A. V. Herzog, and R. C. Dynes, *Phys. Rev. Lett.* **71**, 428 (1993).
- [23] E. Chow, P. Delsing, and D. B. Haviland, *Phys. Rev. Lett.* **81**, 204 (1998).
- [24] D. B. Haviland, K. Andersson, and P. Ågren, *J. Low Temp. Phys.* **118**, 733 (2000).
- [25] D. V. Averin and K. K. Likharev, in *Mesoscopic Phenomena in Solids*, edited by B. L. Altshuler, P. A. Lee and R. A. Webb (Elsevier Science Publishers B. V., Amsterdam, 1991), chap. 6.
- [26] E. Ben-Jacob, K. Mullen, and M. Amman, *Phys. Lett. A* **135**, 390 (1989).

- [27] D. B. Haviland and P. Delsing, Phys. Rev. B **54**, R6857 (1996).
- [28] K. K. Likharev and A. B. Zorin, J. Low Temp. Phys. **59**, 347 (1985).
- [29] M. Watanabe and D. B. Haviland, Phys. Rev. Lett. **86**, 5120 (2001).
- [30] D. B. Haviland, L. S. Kuzmin, P. Delsing, K. K. Likharev, and T. Claeson, Z. Phys. B **85**, 339 (1991).
- [31] L. J. Geerligs, Ph.D thesis, Delft University of Technology (1990).
- [32] Y. Shimazu, T. Yamagata, S. Ikehata, and S. Kobayashi, J. Phys. Soc. Jpn. **66**, 1409 (1997).
- [33] G. Schön and A. D. Zaikin, Phys. Reports **198**, 237 (1990).
- [34] D. B. Haviland, S. H. M. Persson, P. Delsing, and C. D. Chen, J. Vac. Sci. Technol. A **14**, 1839 (1996).
- [35] V. Ambegaokar and A. Baratoff, Phys. Rev. Lett. **10**, 486 (1963); **11**, 104(E) (1963).
- [36] D. B. Haviland, K. Andersson, P. Ågren, J. Johansson, V. Schöllmann, and M. Watanabe, Physica C **352**, 55 (2001).
- [37] M. Watanabe, M. Morishita, and Y. Ootuka, Cryogenics **41**, 143 (2001).
- [38] V. L. Berezinskii, Zh. Eksp. Teor. Fiz. **61**, 1144 (1971) [Sov. Phys. JETP **34**, 610 (1972)].
- [39] J. M. Kosterlitz and D. J. Thouless, J. Phys. C **6**, 1181 (1973).
- [40] G. Falci, R. Fazio, G. Schön, and A. Tagliacozzo, in *Macroscopic Quantum Phenomena and Coherence in Superconducting Networks*, edited by C. Giovanella and M. Tinkham (World Scientific, Singapore, 1996), p. 59.
- [41] S. M. Girvin (private communication).
- [42] U. Geigenmüller and G. Schön, Physica B **152**, 186 (1988).
- [43] G.-L. Ingold and Y. V. Nazarov, in *Single Charge Tunneling*, edited by H. Grabert and M. H. Devoret (Plenum Press, New York, 1992), chap. 2.
- [44] M. Watanabe and D. B. Haviland, J. Phys. Chem. Solids **63**, 1307 (2002).
- [45] M. Watanabe, D. B. Haviland, and R. L. Kautz, Supercond. Sci. Technol. **14**, 870 (2001).
- [46] A. W. Lichtenberger, C. P. McClay, R. J. Mattauch, M. J. Feldman, S.-K. Pan, and A. R. Kerr, IEEE Trans. Magn. **25**, 1247 (1989).
- [47] T. A. Fulton and G. J. Dolan, Phys. Rev. Lett. **59**, 109 (1987).
- [48] J. S. Penttilä, Ü. Parts, P. J. Hakonen, M. A. Paalanen, and E. B. Sonin, Phys. Rev. Lett. **82**, 1004 (1999).